

Prediction of Instability in Rotor-Seal Systems using Forward Whirl Magnetic Bearing Excitation

C. Wagner¹, W. Tsunoda², O. Matsushita³, T. Berninger¹, T. Thümmel¹, D. Rixen¹

To separate different fluids and pressure levels in high-speed turbomachinery or pumps, mostly contactless seals are used. The leakage flow inside the seal gap applies forces to the vibrating rotor system in deflectional and tangential directions, that are dependent on the rotational speed. Above a speed limit, mainly tangential seal forces can lead to self-excited vibrations and, ultimately, rotor instability. This is similar to the “oil whip” phenomenon in journal bearings. To predict the speed limit, two methods are shown and compared: Simulations based on the bulk flow assumptions and an experimental method. To demonstrate the application, a test rig is used. The experimental method uses measured transfer functions, utilizing an active magnetic bearing for forward whirl excitation in the safe operational range. The speed limit can be predicted by analyzing and extrapolating the vibrational behavior of the rotor-seal system.

1 Introduction

Seals in pumps or compressors are used to minimize leakage flow between areas of different pressure levels. Due to the high rotational and relative speeds between rotor and stator in modern turbomachinery, mostly contactless seals like labyrinth, floating ring or gap seals are used. The seal clearance causes a fluid flow through the gap. For an eccentric rotor position, the fluid flow distribution in the gap becomes unsymmetrical and leads to forces on the rotor. These can be modeled similar to additional stiffness, damping and inertia coefficients. The critical speeds can be clearly differentiated compared to the dry rotor ones. This makes dry calculations of the dynamic behavior, like natural frequencies or damping, useless for real operating conditions. The seal gap shown in fig. 1 provides the source of the acting forces, according to Gasch et al. (2006) and Childs (1993).

1. Force pressure velocity relation

The relation between a fluid velocity v and the static pressure is provided by BERNOULLI's equation:

$$p_s = p_t - p_d = p_t - \frac{1}{2}\rho v^2 \quad (1)$$

With the total pressure p_t , the dynamic pressure p_d and the static pressure p_s , which acts on the surface. The integration of the pressure distribution p_s across the rotor surface leads to the acting forces \vec{F} :

$$\vec{F} = \int_A p_s dA \quad (2)$$

2. Restoring force

The restoring LOMAKIN force \vec{F}_L acts against the rotor deflection. It is developed by the axial fluid velocity \vec{u} , which is a pressure-driven POISEUILLE flow, Black and Jenssen (1969). For an ecentered rotor position, the axial fluid flow velocity \vec{u} is higher at the expanded side because of the lower wall-friction influence. This leads to a lower static pressure p_s and a restoring, stiffening force \vec{F}_L , see fig. 1 left. At the seal's entrance, the inlet pressure loss increases this effect and causes the kink of p_s .

3. Destabilizing, deflecting force

Fluid flow in circumferential direction \vec{v} creates the BERNOULLI force \vec{F}_B , which acts in the direction of the rotor eccentricity. The flow is driven by the rotor rotation and evolves into a COUETTE flow for higher seal lengths. Because of mass conservation, the flow speed becomes higher in the narrowed area. This induces a deflecting, destabilizing force \vec{F}_B , see fig. 1 right.

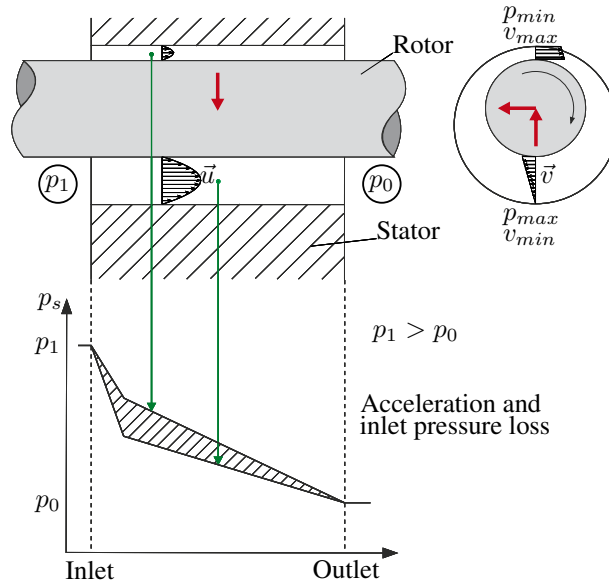


Figure 1: Contactless annular seal, pressure drop and reaction forces, Gasch et al. (2006)

4. Tangential Force

The tangential forces \vec{F}_T pose the highest risk to self-excited rotor vibrations. They act like skew symmetric parts in the stiffness matrix and can induce a rotor instability, similar to the “oil whip” phenomenon in journal bearings, Muszynska (1986). The forces are created by shear stresses between the fluid and the wall, as well as the pressure distribution at the narrowed area of the eccentric rotor.

For a rotordynamic analysis, seals are commonly modeled as a spring-mass-damper system using rotordynamic seal coefficients:

$$-\vec{h}_s = \begin{bmatrix} m_{xx} & 0 \\ 0 & m_{yy} \end{bmatrix} \ddot{\vec{q}} + \begin{bmatrix} c_{xx} & c_{xy} \\ c_{yx} & c_{yy} \end{bmatrix} \dot{\vec{q}} + \begin{bmatrix} k_{xx} & k_{xy} \\ k_{yx} & k_{yy} \end{bmatrix} \vec{q} \quad (3)$$

$\vec{q} = (x \ y)^T$ is the cross deflection (bending) of the rotor, \vec{h}_s is the seal force using the seal coefficients m , c and k for added mass, the fluid’s inertia, damping and stiffness with cross-coupled parts. The cross coupling in the mass matrix is neglected. For the rotordynamic analysis, the various geometries and types of seals are simplified to a plain annular seal.

To calculate critical speeds, vibration amplitudes and rotor instability at the design phase of the machine, validated seal simulation models and experimental methods for component testing are needed. Therefore, two approaches are shown below. The applied simulation models are based on the bulk flow theory and use simplifications made by Black and Jenssen (1969) and Childs (1983) to solve the fluid equations.

To examine the rotordynamic influence of liquid annular seals at the test rig, the authors apply a modern stability diagnosis method that uses measurements in an uncritical speed range to predict the onset speed of instability. The methodology’s origin is the experimental stability diagnosis of oil-film-bearing rotor systems, well described in Matsushita and Fujiwara (2014) and Tsunoda et al. (2016). Here, this method is applied to a flexible rotor with rigid ball-bearing support with plain annular seals. The phenomenology of rotor instability is similar to the journal bearing case. The experimental methodology uses an active magnetic bearing (AMB) as an actor to excite the rotor system. Other investigations using AMB excitation in rotor-seal systems, mainly for coefficient determination, are Kwanka (1999), Gaszner (2015) or Wagner et al. (2016). Another solution for identifying the seal is a levitating AMB-supported rotor, like Zutavern (2006).

In contrast to those, the presented methodology predicts the onset speed of instability to determine the safe operational range of the machinery, using measurements that can be done in the real machine in an uncritical range.

2 Modeling

Here, we provide a brief introduction to the used seal and rotor models. The description of the self-excited rotor vibration phenomenon is based on the work of Muszynska (1986) and Bently et al. (2002). A reduced LAVAL rotor model, according to Gasch et al. (2006), provides the basis to show the model coupling and the seal-rotor behavior.

2.1 Rotor Model

The LAVAL rotor model with a flexible, massless shaft and a symmetrical arranged disk is shown in fig. 2, according to Gasch et al. (2006). The Index I indicates the inertial frame. The disk's center of mass S is displaced by the

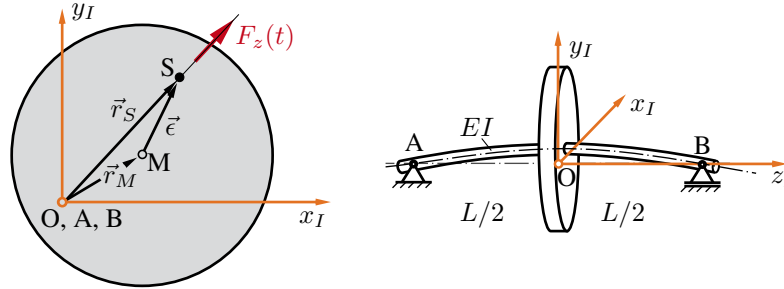


Figure 2: LAVAL rotor model, parametrization to Thümmel et al. (2015) and Roßner (2015)

eccentricity \vec{e} from the geometric center M . The coordinate $q = \vec{r}_M$ is the position of M according to the inertial bearing connection line $A-B$. Substituting $\vec{r}_S = \vec{r}_M + \vec{e}$, the dynamic equilibrium of the rotor can be written with mass m_r and stiffness (bearing and shaft) k_r :

$$\mathbf{M}\ddot{\vec{q}} = \sum_i \vec{F}_i = -\mathbf{K}\vec{q} + \vec{h} \quad (4)$$

$$\begin{bmatrix} m_r & 0 \\ 0 & m_r \end{bmatrix} \ddot{\vec{q}} + \begin{bmatrix} k_r & 0 \\ 0 & k_r \end{bmatrix} \vec{q} = \vec{h} \quad (5)$$

Using $\vec{h} = \vec{h}_u + \vec{h}_e + \vec{h}_s \dots$ (unbalance, external forces, seal forces, etc.) as equivalent forces. The unbalance force with rotational angular frequency Ω of the rotor results in:

$$\vec{h}_u = m_r \vec{e} \Omega^2 \begin{pmatrix} \cos(\Omega t) \\ \sin(\Omega t) \end{pmatrix} \quad (6)$$

The rotor's natural angular frequency is $\omega_{crit} = \sqrt{\frac{k_r}{m_r}}$, its critical speed.

2.2 Seal model

The seal is coupled to the rotor system using forces \vec{h}_s , eq. (3) and fig. 3. As mentioned in the introduction, the rotordynamic seal coefficients are calculated using models and simplifications of the bulk flow theory according to Black and Childs.

Black developed a simple model considering the pressure gradient and the squeeze film. The wall friction is modeled using a constant friction loss factor for both, rotor and stator. Assuming a constant circumferential fluid velocity and neglecting the inertia terms are further simplifications of this model.

Child's model differs in formulating a more complete bulk flow model. The use of semi empirical shear stress formulations for both walls gives the possibility to model different surfaces for rotor and stator (e.g. for damper seals). The fluid's inertia is taken into account to develop the circumferential velocity of the fluid element proceeding along the seal. Further, the inlet swirl (rotational fluid velocity at the seal entrance, see Diewald and Nordmann (1989)) whereas a full developed COUETTE flow is assumed here (due to the long retention time at the rotor surface ahead the seal entrance in our test rig). The detailed description of the theory and the solving process of the fluid equations is well written in Black and Jenssen (1969) and Childs (1983).

The coupled rotor-seal equation of motion is:

$$\begin{bmatrix} m_r + m_{xx} & 0 \\ 0 & m_r + m_{yy} \end{bmatrix} \ddot{\vec{q}} + \begin{bmatrix} c_{xx} & c_{xy} \\ c_{yx} & c_{yy} \end{bmatrix} \dot{\vec{q}} + \begin{bmatrix} k_r + k_{xx} & k_{xy} \\ k_{yx} & k_r + k_{yy} \end{bmatrix} \vec{q} = \vec{h} \quad (7)$$

It is simplified with the assumption of an isotropic, centered rotor using: $M = m_r + m_{xx} = m_r + m_{yy}$, $C = c_{xx} = c_{yy}$, $c = c_{xy} = -c_{yx}$, $K = k_r + k_{xx} = k_r + k_{yy}$ and $k = k_{xy} = -k_{yx}$, (Gasch et al. (2006), p.468 ff.), eq. (7) becomes:

$$\begin{bmatrix} M & 0 \\ 0 & M \end{bmatrix} \ddot{\vec{q}} + \begin{bmatrix} C & c \\ -c & C \end{bmatrix} \dot{\vec{q}} + \begin{bmatrix} K & k \\ -k & K \end{bmatrix} \vec{q} = \vec{h} \quad (8)$$

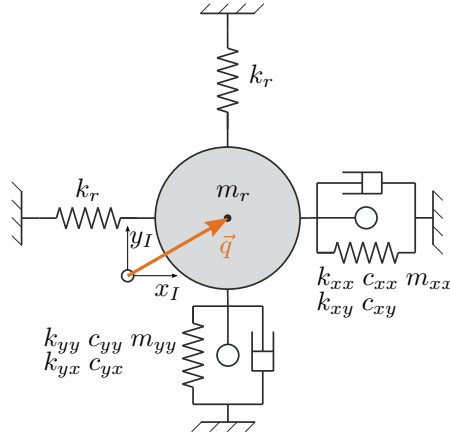


Figure 3: Simplified model: LAVAL rotor coupled to seals

We substitute \vec{q} and \vec{h} with complex coordinates $z = x + jy$ and $F_z = h_x + jh_y$:

$$F_z = M\ddot{z} + C\dot{z} + Kz - j(c\dot{z} + kz) \quad (9)$$

This equation is used to describe the dynamic behavior of the coupled, isotropic LAVAL rotor system.

3 Rotor Instability

A linear oscillation system becomes unstable if the real part of the eigenvalues of the equation of motion becomes positive. The seal coefficients, and eq. (9), are dependent on rotational speed. An eigenvalue analysis of the system for stability analysis is common; $z = \hat{z}e^{\lambda t}$ and $F_z = 0$ are used:

$$M\lambda^2 + C\lambda + K - j(c\lambda + k) = 0 \quad (10)$$

with the eigenvalues $\lambda = \delta + j\omega$:

$$M(\delta + j\omega)^2 + C(\delta + j\omega) + K - j(c(\delta + j\omega) + k) = 0 \quad (11)$$

Instability occurs for $\delta > 0$. This leads to a unstable rotor vibration at the system's first natural frequency. The onset speed of instability is determined at the transition of negative (stable) to positive (unstable) real part δ . At this point, $\delta = 0$ follows:

$$-M\omega^2 + c\omega + K + j(C\omega - k) = 0 \quad (12)$$

Separated into real and imaginary parts:

$$-M\omega^2 + c\omega + K = 0 \quad (\text{quadratic curve}) \quad \wedge \quad C\omega - k = 0 \quad (\text{linear curve}) \quad (13)$$

If both parts of eq. (13) are simultaneously satisfied, so the quadratic and linear curve have a crossing point, the onset speed of instability is reached. Because of the rotational speed dependency of the seal coefficients, this occurs above the speed limit n_{limit} . If the solution for eq. (13) can be found at a stable and safe operating condition, a prediction of n_{limit} is possible. This experimental estimation is done at the test rig and shown in the chapters below.

4 Test Rig: Description and experimental Methodology

The used test rig is shown in fig. 4. It consists of a flexible shaft ⑨ with a mass disk, the seal rotor ② and two stiff ball-bearings ⑥, driven by a servo motor ⑧. The two seals ①, clearance s , are symmetrically arranged to an injection ring ③ in the middle. The fluid is injected and flows through the gaps into the environment. An active magnetic bearing ④ is used as an actuator to excite the system at determined frequencies and whirls. The rotor's movement is detected by two eddy-current sensors ⑤ in the disk's center plain. The seal forces are measured by a piezo dynamometer ⑦ under the seal stator. Furthermore, the fluid temperature, pressure, fluid volume flow and torque are recorded. The dimensions, fluid parameters and operation conditions of the test rig are summarized by

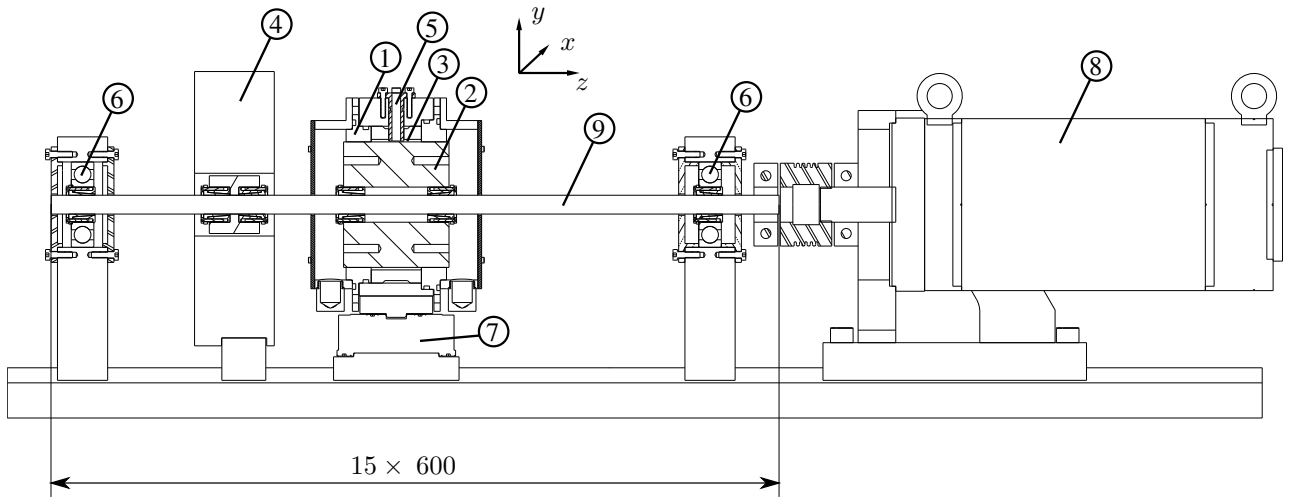


Figure 4: Seal test rig, Wagner et al. (2016)

Table 1: Test rig and fluid parameters

Name	Description	Value
s	clearance seals	0.17 mm
s_i	clearance injection ring	2 mm
n	rot. speed	0 – 6000 rpm
Ω	unbalance angular frequency	1/s
l	seal length	20 mm
l_i	length injection ring	40 mm
Δp	pressure drop at the seal	$2 \cdot 10^5$ Pa
ν	kinematic viscosity at 40°C	$4.05 \cdot 10^{-2}$ Pa · s
ρ	density at 40°C	880 kg/m ³
d	diameter seal rotor	0.1 m
m_r	mass disk	5 kg
k_r	shaft stiffness	$2.93 \cdot 10^5$ N/m
ω_0	“dry” 1.natural frequency	38.6 Hz

table 1.

Figure 5 shows the run-up response of the rotor-seal system. Compared to the seal-less system, whose behavior is like an ideal LAVAL rotor, the seal dominates the system dynamics. The unbalance response looks like an overdamped system with a first natural frequency at about half the rotational speed. Due to this, the rotor is always in an overcritical range.

This measurement result shows a strong rotational speed depending of the first natural frequency, induced by the rotational speed dependency of the rotordynamic seal coefficients $m(n), c(n), k(n)$.

5 Prediction of Rotor Instability

To predict the speed limit at the instability, two methods are shown. The first one uses the eigenvalue calculation of simulated seal coefficients. The second one is an experimental method, which uses a separation, a CO-QUAD analysis, and a zero-crossing search of the measured frequency response function $G(\omega)$ at stable operating points.

5.1 Simulation: Eigenvalue Analysis

Using the coupled equation of motion (7) and simulated seal coefficients, the eigenvalues $\lambda = \delta \pm j\omega$ can be calculated for a stability analysis according to the rotational speed. Figure 6 shows the plots of the eigenvalues of

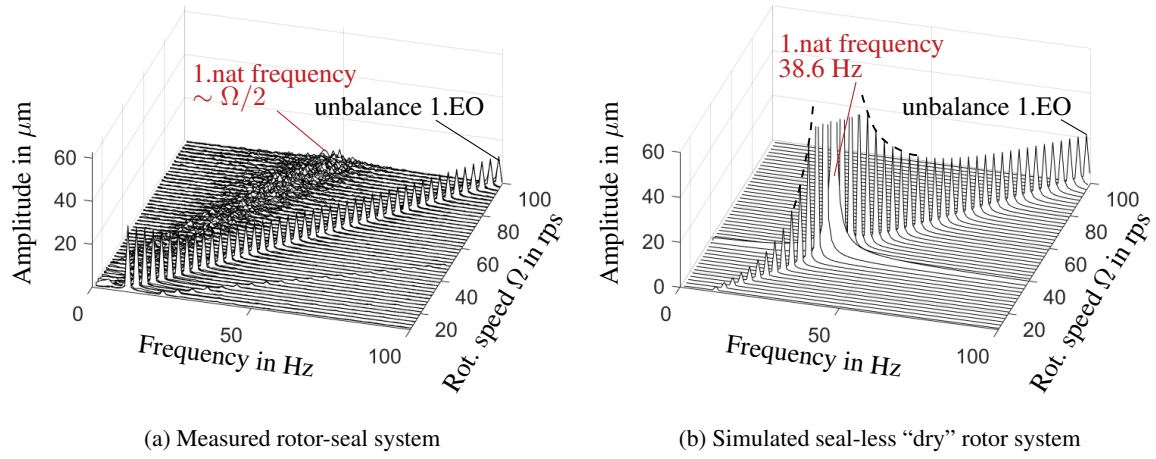


Figure 5: 3D-Campbell diagram of the test rig

the system for two implemented simulation models, Black and Jenssen (1969) and Childs (1983) model. The zero crossing of the real part δ detects the onset speed of instability to $n_{limit} = [160 \text{ and } 124] \text{ rps}$ for the two models. The imaginary part, the natural frequency, shows a strong rotational speed dependency, like the measurement in fig. 5. It is about $\Omega/2$ at the stability limit. The simulation results are just used for verification of the experimental

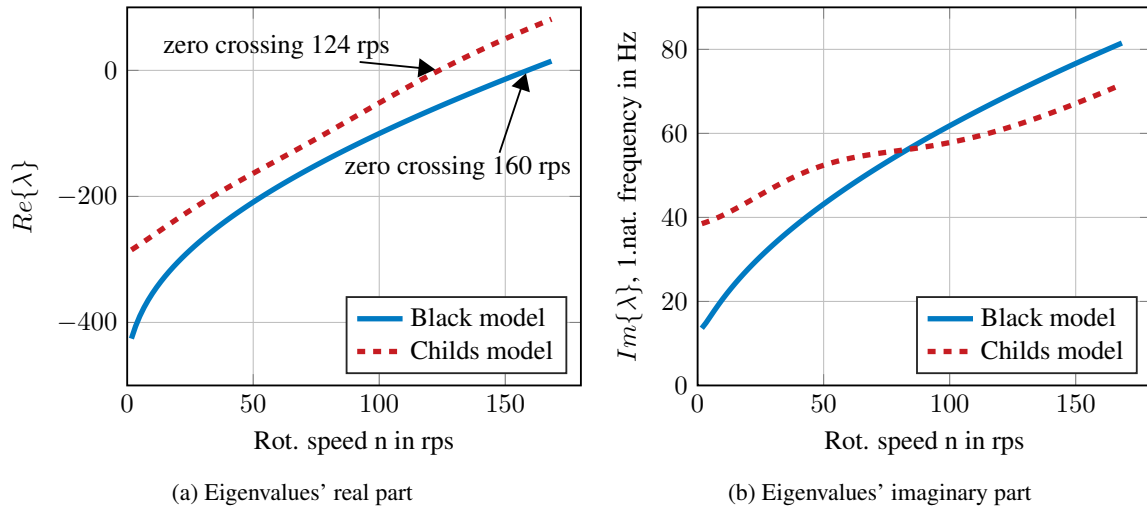


Figure 6: Eigenvalue analysis of the simulated rotor-seal system

methodology. At this point, the test rig cannot reach the instability due to rotational speed restrictions.

5.2 Experimental Methodology: Co-Quad Analysis

Using the measured rotor displacement in frequency domain $\hat{z}(\omega)$, rotor response, and the exciting force (forward whirl with AMB) $\hat{F}_z(\omega)$, the transfer function (TF) $G(\omega)$ can be calculated according to the model eq. (9):

$$G(\omega) = \frac{\hat{z}}{\hat{F}_z} = \frac{1}{-M\omega^2 + c\omega + K + j(C\omega - k)} \quad (14)$$

Separated into real and imaginary parts, in CO-QUAD form:

$$\text{Re}\{G(\omega)\} = \frac{-M\omega^2 + c\omega + K}{(-M\omega^2 + c\omega + K)^2 - (C\omega - k)^2} \quad (15)$$

$$\text{Im}\{G(\omega)\} = \frac{-C\omega + k}{(-M\omega^2 + c\omega + K)^2 - (C\omega - k)^2} \quad (16)$$

The plots of the measured TF separated into real and imaginary parts are shown in fig. 7. The solution for eq. (13) is the zero crossing of both parts, ($Re\{G(\omega)\}$ and $Im\{G(\omega)\}$), at the same frequency ω . At this point, the denominator of eq. (14) becomes zero, so the amplitude \hat{z} arises and the instability occurs.

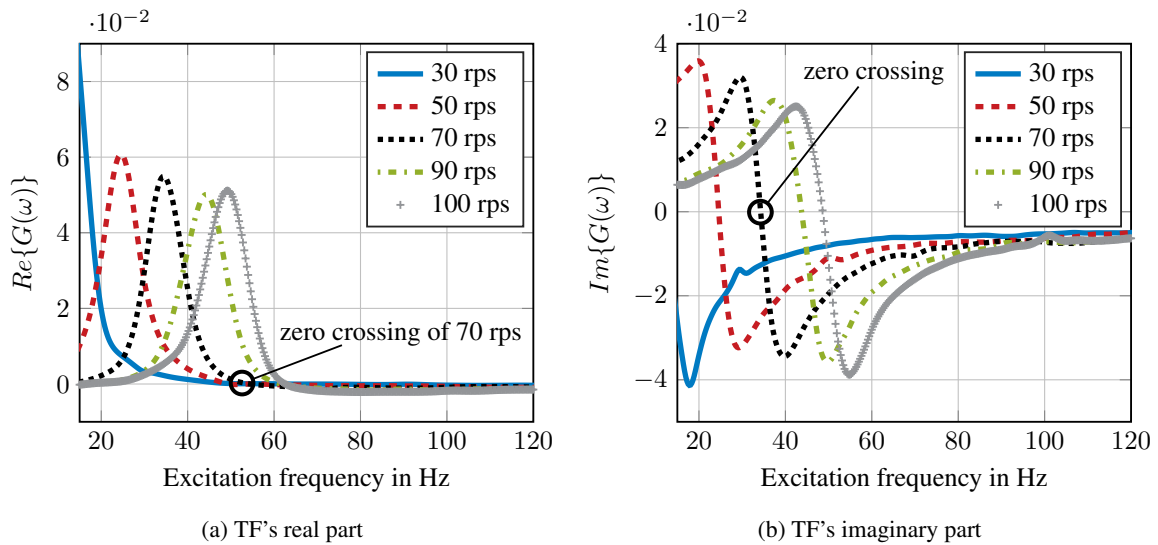


Figure 7: Measured TF $G(\omega)$ of the test rig as a CO-QUAD plot

Therefore, at constant rotational speed n , the system becomes excited in a forward whirl direction with AMB at several frequencies ω and the TF $G(\omega)$ is calculated using discrete Fourier transformation. Then, the zero crossing of the real and imaginary parts at every rotational speed must be found. These zero-crossing frequencies show almost linear behavior according to the rotational speed, see fig. 8. The zero-crossing points of the real part are the undamped natural frequency and are nearly constant. The imaginary ones increase linearly with the rotational speed.

This occurs because the tangential forces, the cross-coupled parts in the stiffness matrix, are responsible for the instability. These forces are created by shear stresses between the fluid and the wall, depending on the velocities in circumferential direction, which are almost linear to the rotational speed (COUETTE flow assumption).

When both curves cross, the denominator of eq. (14) becomes zero, eq. (13) is fulfilled and the instability occurs. A linear fit of the graphs with extrapolation, using the least squares method, provides the crossing, and the instability can be predicted to $n_{limit} = 122$ rps.

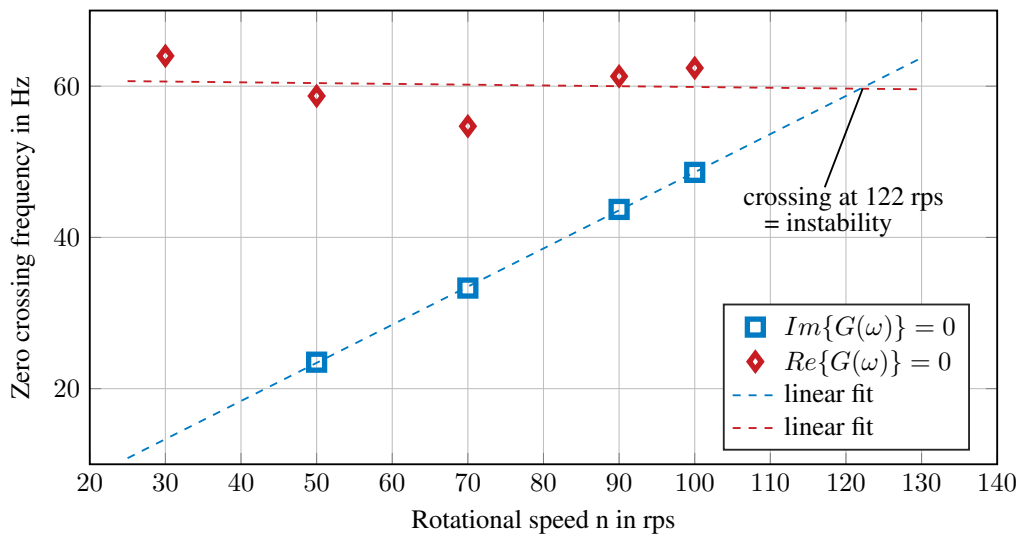


Figure 8: Zero crossing of the real and imaginary parts of the measured TF $G(\omega)$ and prediction of stability limit using linear fit and extrapolation

6 Conclusion

This article examines the influence of contactless seals on rotor systems. The rotor instability phenomenon as well as a simulative and an experimental methodology to predict the speed limit are shown. The experimental prediction method uses transfer function measurements, curve fitting and extrapolation at a safe, low-speed range. The measured transfer functions at several rotating speeds are separated into real and imaginary parts and a CO-QUAD analysis is done to identify the zero crossing frequencies. Plotting the zero points of the real and imaginary parts according to the rotational speed, one can predict the onset speed of instability. The comparison between the simulation and the experimental-based prediction shows 24% for the Black simulation model and 1.6% discrepancy for the Childs. Future works will include increasing the test rig's rotational speed until instability as well as the validation of the simulation model and the experimental prediction methodology.

7 Acknowledgment

This project is supported by the Ludwig Bölkow Campus and the Bavarian State. The good cooperation between the partners within the research project is well appreciated.

References

- Bently, D. E.; Hatch, C. T.; Grissom, B.: *Fundamentals of rotating machinery diagnostics*. Bently Pressurized Bearing Press (2002).
- Black, H.; Jenssen, D.: *Dynamic Hybrid Bearing Characteristics of Annular Controlled Leakage Seals*. Proceedings of the Institution of Mechanical Engineers; SAGE Publications Sage UK, London, England (1969).
- Childs, D. W.: Dynamic Analysis of Turbulent Annular Seals Based On Hirs' Lubrication Equation. *ASME, Lubrication Technology*, 105, (1983), 429–436.
- Childs, D. W.: *Turbomachinery Rotordynamics*. Wiley-Interscience, Dallas, TX, USA (1993).
- Diewald, W.; Nordmann, R.: Dynamic Analysis of Centrifugal Pump Rotors With Fluid-Mechanical Interactions. *Journal of Vibration Acoustics Stress and Reliability in Design*, 111, 4, (1989), 370.
- Gasch, R.; Nordmann, R.; Pfützner, H.: *Rotordynamik*. Springer (2006).
- Gaszner, M.: *Rotordynamische Charakterisierung von Dichtungssystemen zur Anwendung in Kraftwerksdampfturbinen*. Ph.D. thesis, Technical University of Munich (2015).
- Kwanka, K.: *Dynamic Coefficients of Stepped Labyrinth Gas Seals*, vol. 122. *Journal of Engineering for Gas Turbines and Power* (1999).
- Matsushita, O.; Fujiwara, H.: *Rotordynamics in HIL and Vibrational diagnostic technics*. v_BASE forum, Tokyo, Japan (2014).
- Muszynska, A.: *Whirl and whip-Rotor/bearing stability problems*, vol. 110. *Journal of Sound and Vibration* (1986).
- Roßner, M.: *Modellbasiertes Monitoring von Rotoren mit mehreren gleichzeitigen Fehlern*. Ph.D. thesis, Technical University of Munich (2015).
- Thümmel, T.; Roßner, M.; Ulbrich, H.; Rixen, D.: *Unterscheidung verschiedener Fehlerarten beim modellbasierten Monitoring*. Proceedings SIRM2015 - 11. Internationale Tagung Schwingungen in Rotierenden Maschinen (2015).
- Tsunoda, W.; Hijikata, W.; Shinshi, T.; Fujiwara, H.; Matsushita, O.: *Diagnostic experiments for stability of rotor-oil film bearing systems using radial magnetic bearing excitation*. *Vibrations in Rotating Machinery (VIRM 11) Conference*, Manchester, UK. (2016).
- Wagner, C.; Berninger, T.; Thümmel, T.; Rixen, D.: *Rotordynamic Effects in Turbopumps for Space Propulsion Systems - First Minimal Models and Experimental Validation*. *Space Propulsion 2016 Conference*, 3AF, Rome, Italy (2016).

Zutavern, Z. S.: *Identification of Rotordynamic Forces in a Flexible Rotor System Using Magnetic Bearings Identification of Rotordynamic Forces in a Flexible Rotor System Using Magnetic Bearings*. Ph.D. thesis, Texas (2006).

Address: ¹ Chair of Applied Mechanics, Technical University of Munich, Boltzmannstr. 15, 85748 Garching
email: {c.wagner, t.berninger, thuemmel, rixen}@tum.de

² Department of Mechanical Engineering, Tokyo Institute of Technology, 4259, Nagatsuta-cho, Midori-ku, 226-8503 Yokohama, Japan

email: tsunoda.w.aa@m.titech.ac.jp

³ Department of Mechanical Engineering, National Defense Academy, 1-10-20 Hashirimizu, 239-8686 Yokosuka, Japan

email: osami@tiger.odn.ne.jp